DNA Damage Stress Control Is a Truncated Large T Antigen and Euchromatic Histone Lysine Methyltransferase 2–Dependent Central Feature of Merkel Cell Carcinoma

Kamel Bachiri, Diala Kantar, Estelle M.N. Laurent, Pauline Gaboriaud, Laurine Durand, Aurélie Drouin, Mélanie Chollot, David Schrama, Roland Houben, Thibault Kervarrec, et al.

HAL Id: hal-04666767
https://hal.inrae.fr/hal-04666767v1

Submitted on 2 Aug 2024

DNA Damage Stress Control Is a Truncated Large T Antigen and Euchromatic Histone Lysine Methyltransferase 2−Dependent Central Feature of Merkel Cell Carcinoma

*JID*Open

Kamel Bachiri[1,6], Diala Kantar[1,6], Estelle M.N. Laurent[1], Pauline Gaboriaud[2], Laurine Durand[2], Aurélie Drouin[2], Mélanie Chollot[3], David Schrama[4], Roland Houben[4], Thibault Kervarrec[2,5], Laetitia Trapp-Fragnet[3], Antoine Touzé[2,7] and Etienne Coyaud[1,7]

Merkel cell carcinoma (MCC) is an aggressive skin cancer with a high mortality rate. Merkel cell polyomavirus causes 80% of MCCs, encoding the viral oncogenes small T and truncated large T (tLT) antigens. These proteins impair the RB1-dependent G1/S checkpoint blockade and subvert the host cell epigenome to promote cancer. Whole-proteome analysis and proximal interactomics identified a tLT-dependent deregulation of DNA damage response (DDR). Our investigation revealed, to our knowledge, a previously unreported interaction between tLT and the histone methyltransferase EHMT2. T antigen knockdown reduced DDR protein levels and increased the levels of the DNA damage marker γH2Ax. EHMT2 normally promotes H3K9 methylation and DDR signaling. Given that inhibition of EHMT2 did not significantly change the MCC cell proteome, tLT−EHMT2 interaction could affect the DDR. With tLT, we report that EHMT2 gained DNA damage repair proximal interactors. EHMT2 inhibition rescued proliferation in MCC cells depleted for their T antigens, suggesting impaired DDR and/or lack of checkpoint efficiency. Combined tLT and EHMT2 inhibition led to altered DDR, evidenced by multiple signaling alterations. In this study, we show that tLT hijacks multiple components of the DNA damage machinery to enhance tolerance to DNA damage in MCC cells, which could explain the genetic stability of these cancers.

Keywords: DNA damage repair signaling, EHMT2, Merkel cell carcinoma, Proteome analysis, Proximal interactomics, Truncated LT

INTRODUCTION

Merkel cell carcinoma (MCC) is a rare and very aggressive neuroendocrine carcinoma of the skin (Becker et al, 2018). This neoplasia has a worse prognosis than other skin cancers, even matching that of advanced-stage melanoma (Becker

et al, 2018). The main risk factors for MCCs are aging, UV exposure, and immunosuppression (Heath et al, 2008). In 2008, Feng et al (2008) established a viral etiology for 80% of MCC cases. The conjunction of 2 rare events leads to the emergence of these virus-positive MCC (VP-MCC): (i) the viral genome integration and (ii) a truncation before the large T antigen (TA) helicase domain by mutation or integration. The small TA (sT) and a truncated large TA (tLT) drive VP-MCC transformation, survival, and growth (Houben et al, 2012; Shuda et al, 2014). Furthermore, VP-MCCs display a very low mutational burden (0.4 per Mb) compared with their virus-negative MCC counterparts (40 per Mb), which are related to UV exposure, highlighting TA-driving functions in VP-MCC oncogenesis (Goh et al, 2016). Merkel cell polyomavirus (MCPyV) has been detected in other cancers as well. However, not only is the observed viral load lower in these cases, but also—in contrast to MCC—demonstration of a contribution of MCPyV to tumorigenesis is lacking (Silling et al, 2022).

MCPyV TAs are thought to profoundly impact VP-MCCs mainly through cell-cycle checkpoint inhibition and epigenetic reprogramming. The canonical mechanism of tLT in VP-MCC oncogenesis is the sequestration of RB1. Although this mechanism is essential to maintain cancer growth, it does not fully explain the MCC phenotype. Despite that several

ARTICLE IN PRESS

K Bachiri et al.
DNA Damage Control by tLT and EHMT2 Is Central in MCC

Merkel cell markers are expressed by MCCs, recent studies suggest an epithelial precursor origin (Gravemeyer et al, 2022; Kervarrec et al, 2020a; Kervarrec, 2022). The Merkel cell phenotypic markers are believed to be acquired through epigenetic and transcriptional remodeling (Kervarrec et al, 2020b). Several mechanisms connect TAs to epigenetic reprogramming, for example, transcriptional activation through sT-dependent MYC-L recruitment to EP400 (Cheng et al, 2017). EP400-sT triggers additional epigenetic changes, such as sT—MYCL—EP400 complex driving the transcriptional activation of LSD1, a histone demethylase that represses ATOH1 target expression, which in turn prevents differentiation (Leiendecker et al, 2020; Park et al, 2020). Furthermore, EZH2 (a PRC2 subunit) inhibition slows down MCC xenograft development through *SIX1* derepression (Gartin et al, 2022). This effect results from the TA-driven overexpression of EZH2, thus allowing for a selective toxicity of EZH2 inhibition in VP-MCC cell lines (Durand et al, 2023).

Given the recent evidence positioning histone methylation processes at the core of VP-MCC oncogenesis (LSD1, EZH2), we mined our tLT interactomics data for methylation-related factors and selected euchromatic histone lysine methyl-transferase (EHMT) 2. EHMT2 is an epigenetic writer assembling in an EHMT1—EHMT2—WIZ complex (Tachibana et al, 2002; Ueda et al, 2006). This complex decorates H3K9me1/2 (histone H3 Lysine 9 mono and dimethylation), leading to transcriptional repression of neighboring loci (Tachibana et al, 2002). EHMT2 is also involved in monomethylation of H3K27 (Wu et al, 2011) and, beyond its role in transcriptional regulation, can prime proliferating cell nuclear antigen (PCNA) docking for replication through H3K56me1 (Yu et al, 2012). Several studies localize EHMT2 near replication forks, notably through BioID identification of PCNA interactors and the innovative iPond technique that identifies proteins linked to nascent DNA (Sirbu et al, 2013; Srivastava et al, 2018). The methylation of H3K9 by EHMT2 has been linked to DNA damage in several studies (Ayrapetov et al, 2014; Ginjala et al, 2017). For example, it was recently reported that EHMT2 ensures a protective function in replication stress—induced DNA damage. In this regard, EHMT2 methyltransferase activity is associated with trimethylation of H3K9 near stalled forks, leading to a protective chromatin compaction state (Gaggioli et al, 2023).

EHMT2 can also methylate substrates involved in DNA damage response (DDR) regulation. One of the few described mechanisms in this pathway is the dimethylation of p53$_{K373}$ (Huang et al, 2010). This modification prevents the inactive form of p53 from becoming active. This phenotype is reversed by the downregulation of EHMT2, leading to p53 activation and apoptosis. In closer relation to the DDR, MDC1 has been observed to be methylated by EHMT2 on K45, promoting the interaction between MDC1 and ataxia telangiectasia mutated (ATM), resulting in increased ATM activation (Watanabe et al, 2018).

In this study, we reveal that EHMT2 is addressed at the proximity of DNA damage sites by tLT and is involved in TA depletion—mediated cell death. In a broader view, we show that the EHMT2 methyltransferase activity is central in the

DDR and provide strong insights that MCC oncogenesis also relies on tLT-driven DNA damage and DDR control.

RESULTS

TA expression is associated with increased expression of proteins involved in replication and DNA damage machineries

To explore the role of the TAs in established MCC cells, we first analyzed the whole proteome of WaGa cells (VP-MCC cell line) and assessed the changes induced by short hairpin RNA (shRNA)—mediated repression of TA expression. To this end, WaGa cells carrying a doxycycline (Dox)-inducible TA shRNA and wild-type (WT) WaGa were harvested after 7 days in the presence of Dox, and their protein content was analyzed by tandem mass spectrometry coupled with liquid chromatography.

Expectedly, we detected a fivefold decrease of tLT in Dox-treated WaGa cells with inducible TA shRNA knockdown; we were not able to quantify the changes in abundance of sT because all the peptides identified were common between sT and tLT and were assigned to tLT during the analysis (Supplementary Table S1). In addition, we identified 101 overexpressed proteins (72 upregulated >2-fold and 29 exclusively expressed upon TA knockdown) and 150 proteins with reduced/undetectable expression upon shRNA induction (110 downregulated >2-fold and 40 exclusive to WT) (Figure 1a and b). Among those higher expressed proteins in the presence of MCPyV TA, we identified all the components of the replication factor C complex, 2 of the mini-chromosome maintenance protein complex (MCM2/6), and the 8 subunits of the condensin complex. Furthermore, 24 proteins annotated as involved in replication and 25 in DNA
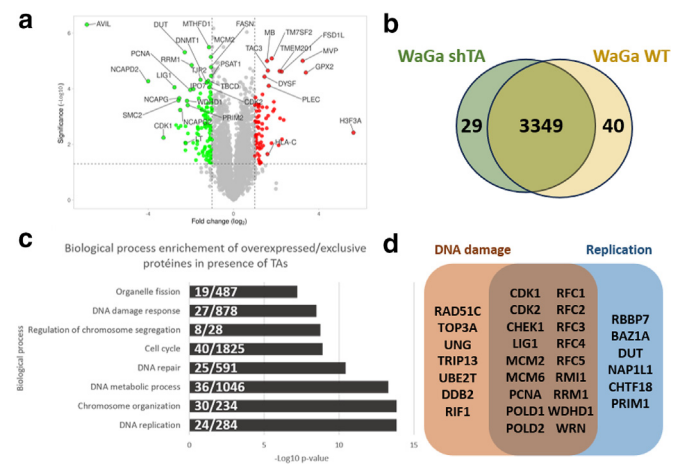
Figure 1. Differential protein expression in the presence and absence of TAs. (**a**). Volcano plot presenting proteins for which expressions significantly changed after TA shRNA-mediated knockdown ($P < .05$; log$_2$ fold change >1 or < −1). (**b**). Number of proteins identified in both conditions with valid values in all 3 replicates (29 and 40 are unique to WaGa shTA and WaGa WT, respectively). (**c**). BP enrichment analysis of proteins overexpressed in the presence of TAs. The graphic displays the number of proteins identified for each GO BP along with the total number of proteins annotated in the GO term. (**d**). Proteins overexpressed in the presence of TAs that are annotated to be involved in replication and/or DNA damage response. BP, biological process; GO, Gene Ontology; shRNA, short hairpin RNA; shTA, T antigen—targeted short hairpin RNA; TA, T antigen; WT, wild-type.

ARTICLE IN PRESS

K Bachiri et al.
DNA Damage Control by tLT and EHMT2 Is Central in MCC

repair were more abundant in the presence of MCPyV TA (Figure 1c and d). For example, we could identify RIF1 and RAD51C, which are both involved in homologous junction and genetic instability control. The finding that the MCPyV TAs drive an upregulation of DNA replication factors is not surprising given that MCC cell lines are addicted to TAs for growth (Houben et al, 2012). However, the induction of DDR components when MCPyV TA is present suggests an enhanced DNA repair capacity, which could provide a mechanistic insight toward the low mutation burden and the genetic stability of MCC cells.

Because the Dox-induced growth reduction in the WaGa cells with inducible TA shRNA knockdown can be completely rescued by re-expression of only tLT (Angermeyer et al, 2013), the most crucial effects of the TA shRNA in this experimental system seem to be mediated by targeting tLT expression. Therefore, in the following sections, we focused on tLT.

tLT proximal interactome uncovers epigenetic regulators potentially driving specific MCC features

To characterize a putative link between tLT and the DNA damage control machinery, we used human embryonic kidney (HEK) 293 cells as model system and delineated the putative proximal protein landscape of 330 amino acids tLT (representing the tLT expressed in the MCC cell line MKL-1) using BioID (Roux et al, 2012). After stringent filtering and background removal, we identified 363 high-confidence tLT proximal interactors (Supplementary Table S2). Importantly, we retrieved most of the known interactors of tLT, including the interactions with RB1 and heat shock proteins (Cheng et al, 2017; Houben et al, 2012; Kwun et al, 2015), demonstrating the reliability of our approach. Indeed, we identified several proximal interactions with chaperone proteins from the Hsc70 family for which an interaction domain has been identified in the amino terminus of large T antigens (An et al, 2012). Over 80% of the identified interactors are nuclear proteins, highlighting the prominent role of tLT in nuclear mechanisms. Gene Ontology term analysis identified 3 highly enriched categories, that is, proteins involved in RNA structure and stability, in transcription regulation and in epigenetic remodeling. The presence of 66 proteins involved in epigenetic regulation through histone modification stresses the importance of epigenetic remodeling in MCC (Figure 2). Among them, we detected most of the components of the nucleosome remodeling and deacetylase (NuRD) complex and the complete deacetylase subcomplex. tLT is also found in proximity to BEND3, establishing a putative link between NuRD and PRC2, already known to be involved in MCCs through EZH2 (Durand et al, 2023; Gartin et al, 2022). Interestingly, the proximal interactome of tLT unveiled an important number of proteins regulating histone and DNA methylation. Focusing on this modification, we identified tLT at proximity of the writer complex EHMT2, euchromatic histone lysine methyltransferase 1, and WIZ along with the eraser KDM3B, both regulating the methylation state of H3K9. Interestingly, the enrichment analysis of the interactors using a combination of Gene Ontology tools, gProfiler, WebGestalt, and enrichR, also revealed a significant enrichment of proteins involved in DDR such as TP53BP1,
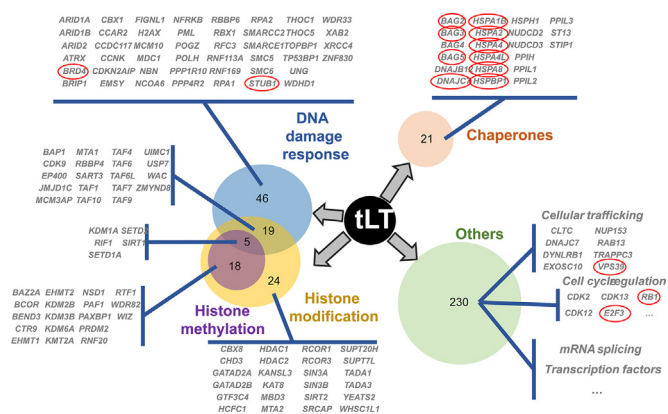

Figure 2. tLT proximal interactors sorted by biological process. The BioID-based tLT proximal interactors are sorted by the most enriched biological processes of the interactome. Red circles depict the known interactors for tLT in our dataset. The complete list of interactors is available in Supplementary Table S1. tLT, truncated large T antigen.

TOPBP1, MDC1, RPA1-2, RFC3, or XRCC4 (Karatzas et al, 2023).

Inhibition of EHMT2 methyltransferase activity has no impact on the proteome of VP-MCC cells

Because EHMT2 had the highest label-free quantification values among the methyltransferases in tLT BioID, we assessed the putative proteome remodeling after its inhibition. We first determined the half-maximal inhibitory concentration of BRD4770, a validated inhibitor of EHMT2 methyltransferase activity (Supplementary Material and Methods and Supplementary Figure S1). We noted that VP-MCCs were more resistant to EHMT2 inhibition than the melanoma cell line A375 or the HEK cell line HEK293, suggesting an important role of EHMT2 specifically in VP-MCCs. To test the impact of EHMT2 inhibition on protein expression in TA-expressing cells, WaGa cells with and without TA knockdown were treated with 5 μM BRD4770 (in the half-maximal inhibitory concentration range) for 48 hours, and their proteomes were analyzed by mass spectrometry. Surprisingly, we did not observe significant proteome changes after 48 hours of EHMT2 chemical inhibition, neither in the presence nor in the absence of tLT (Supplementary Table S3), suggesting a role of EHMT2 independent of its ability to regulate transcription.

tLT does not disrupt the basal interactome of EHMT2 but brings it at the vicinity of stalled forks and DDR factors

After validation of the tLT–EHMT2 interaction by proximity ligation assay in 2 VP-MCC cell lines (MKL-1 and WaGa) (Figure 3a–d), we tested the impact of tLT on the proximal interactome of EHMT2. EHMT2 BioID in basal conditions in HEK293 cells identified 136 high-confidence proximal interactors for EHMT2. A total of 89% of these interactions were conserved in the presence of tLT, in line with the absence of proteome changes after EHMT2 inhibition with/without tLT.

Strikingly, when compared with the controls, we detected a strong gain of proximal interactors (Supplementary Table S4). This increase in the number of interactors suggests an addressing of EHMT2 at additional diversified loci on

ARTICLE IN PRESS

K Bachiri et al.
DNA Damage Control by tLT and EHMT2 Is Central in MCC
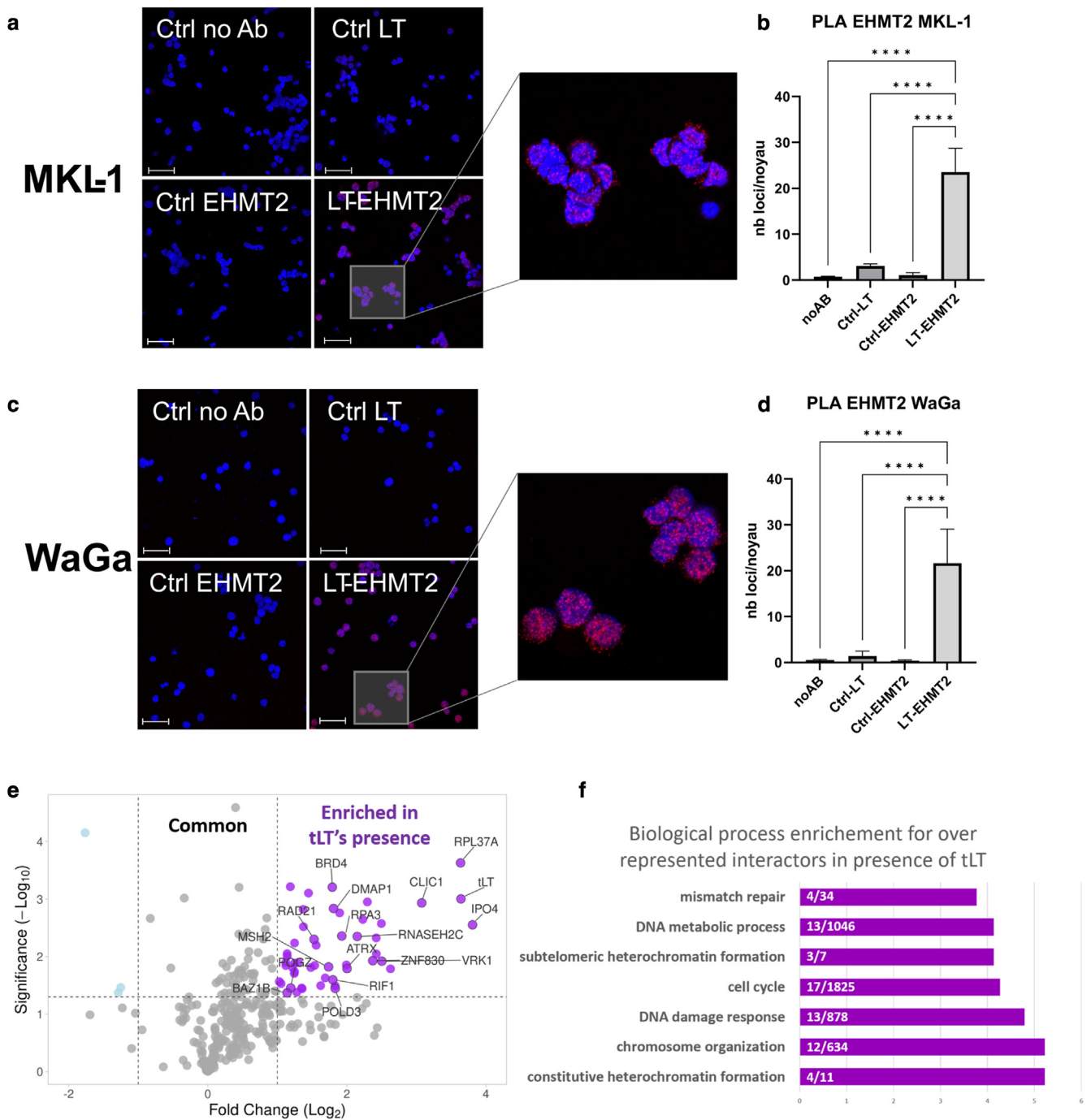
Figure 3. EHMT2 proximal interactors with and without expression of tLT and the biological processes enriched. (**a**) Confocal image of proximity ligation assay between EHMT2 and tLT in MKL-1 cells. Bar = 50 µm. (**b**) Number of fluorescence foci per nuclei. (**c**) Confocal images of proximity ligation assay between EHMT2 and tLT in WaGa cells. Bar = 50 µm. (**d**) Number of fluorescence foci per nuclei. (**e**) Volcano plot depicting the interactors identified for EHMT2 in presence of tLT versus in absence of the viral protein. The proteins in the top right area are the ones significantly enriched in the presence of tLT ($P < .05$). (**f**). GO biological process enrichment analysis of the 50 proteins significantly enriched in EHMT2's interactome in the presence of tLT. Ctrl, control; EHMT2, euchromatic histone lysine methyltransferase 2; GO, Gene Ontology; tLT, truncated large T antigen.

the chromatin through interaction with tLT. Indeed, comparing the 2 EHMT2 proximal interactomes with/without tLT, we identified 50 factors significantly enriched in the presence of tLT (Figure 3e).

Surprisingly, >25% of these proteins are involved in DNA damage regulation (Figure 3f). tLT-dependent proximity of EHMT2 with proteins such as RPA3 allows us to narrow down

the presence of EHMT2 at DDR sites and connect it to replication stress and single-strand break (SSB)–related processes. EHMT2 has been observed in the environment of DDR through PCNA interactome identification (Srivastava et al, 2018). EHMT2 can methylate several nonhistone proteins. Among the possible targets of EHMT2, we detected MDC1, for which the methylation is required for proper local

ARTICLE IN PRESS

K Bachiri et al.
DNA Damage Control by tLT and EHMT2 Is Central in MCC

activation of phosphorylated ATM. However, the interaction between EHMT2 and MDC1 is detected both with/without tLT and does not seem to be influenced by its presence.

To explore the importance of the EHMT2−tLT interplay, we then combined their inhibition in VP-MCC cell lines.

EHMT2 inhibition rescues tLT depletion−dependent MCC cell death and protects against DNA damage

After assessment of efficient shRNA-mediated knockdown in the VP-MCC cell lines (Supplementary Figure S2), proliferation assays were performed on WT versus WaGa cells with inducible TA shRNA knockdown, MKL-1 (Figure 4a and b), and PeTa (Supplementary Figure S3a). In line with previous results (Hesbacher et al, 2016), the WaGa cells with inducible TA shRNA knockdown demonstrated, after 7 days of Dox treatment, decreased proliferation compared with their corresponding parental controls treated with Dox, as assayed by tetrazolium inner salt assay. However, treatment with increasing doses of the EHMT2 inhibitor BRD4770 for 48 hours after 5 days of shRNA induction led to reduced growth inhibition, whereas in the parental VP-MCC cell lines, the inhibitor decreased proliferation. Thus, the inhibition of EHMT2 in WaGa, MKL-1, and PeTa inducible TA shRNA is able to partially rescue the cells from cell cycle arrest upon TA knockdown and to restore proliferation. These results were further confirmed using mixed culture assay of WaGa GFP and WaGa cells with inducible TA shRNA knockdown (Figure 4c). We measured the ratio of WaGa cells with inducible TA shRNA knockdown/WaGa GFP and observed an inversion of the curves upon EHMT2 inhibition at the sixth day in the presence of Dox, and this ratio keeps increasing over time. Considering the previous results, it is possible that in the absence of TAs, the lack of EHMT2 methyltransferase activity precludes an efficient DDR and/or cell cycle checkpoints signaling. We measured cell proliferation in WaGa with/without TAs depletion treated with various concentrations of etoposide, a topoisomerase 2 inhibitor, and EHMT2 inhibitors BRD4770 and UNC0642 (Figure 4d). Again, we observed the rescue of the cells depleted in TAs by EHMT2 inhibition with BRD4770 and UNC0642. Interestingly the inhibition of EHMT2 led to better viability after the treatment with etoposide, which is correlated to a decreased number of γH2Ax foci in WaGa cells with inducible TA shRNA knockdown (Figure 5a and b). In this experiment, we counted the number of γH2Ax foci formed by the cells expressing TAs or not, under EHMT2 inhibition and/or in the presence of etoposide (Figure 5a and b).

In parental WaGa cells, γH2Ax foci indicating DNA damage were induced by treatment with etoposide, and this response was observed to be even stronger in the WaGa cells with inducible TA shRNA knockdown (Figure 5a and b). Surprisingly, the treatment with the EHMT2 inhibitor
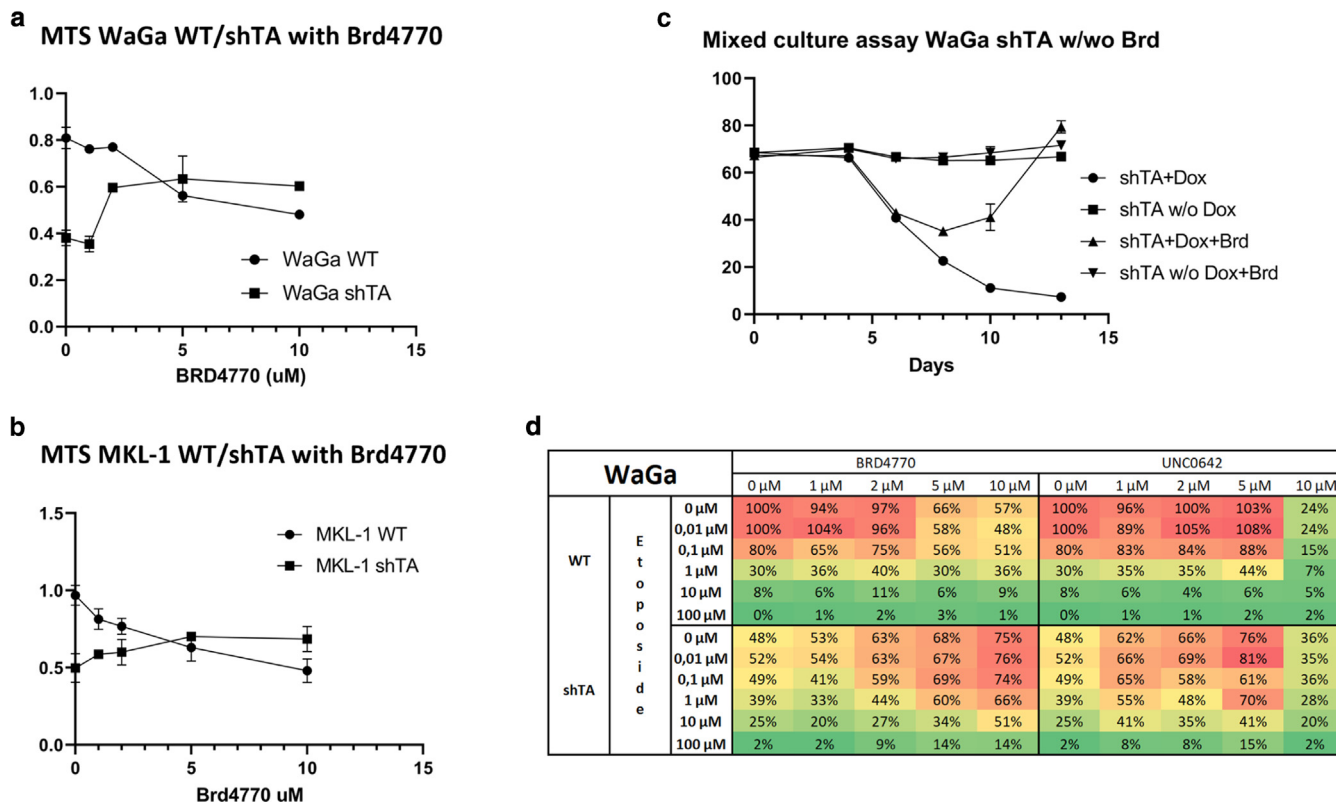

a MTS WaGa WT/shTA with Brd4770

b MTS MKL-1 WT/shTA with Brd4770

c Mixed culture assay WaGa shTA w/wo Brd

d

WaGa			BRD4770					UNC0642				
			0 µM	1 µM	2 µM	5 µM	10 µM	0 µM	1 µM	2 µM	5 µM	10 µM
WT	E t o p o s i d e	0 µM	100%	94%	97%	66%	57%	100%	96%	100%	103%	24%
		0,01 µM	100%	104%	96%	58%	48%	100%	89%	105%	108%	24%
		0,1 µM	80%	65%	75%	56%	51%	80%	83%	84%	88%	15%
		1 µM	30%	36%	40%	30%	36%	30%	35%	35%	44%	7%
		10 µM	8%	6%	11%	6%	9%	8%	6%	4%	6%	5%
		100 µM	0%	1%	2%	3%	1%	0%	1%	1%	2%	2%
shTA		0 µM	48%	53%	63%	68%	75%	48%	62%	66%	76%	36%
		0,01 µM	52%	54%	63%	67%	76%	52%	66%	69%	81%	35%
		0,1 µM	49%	41%	59%	69%	74%	49%	65%	58%	61%	36%
		1 µM	39%	33%	44%	60%	66%	39%	55%	48%	70%	28%
		10 µM	25%	20%	27%	34%	51%	25%	41%	35%	41%	20%
		100 µM	2%	2%	9%	14%	14%	2%	8%	8%	15%	2%

Figure 4. EHMT2 inhibition's effect on VP-MCC cells viability with and without tLT. (**a, b**) Viability of the cells was assessed by MTS assay after 48 hours of treatment with EHMT2 inhibitor at different concentrations in (**a**) WaGa or (**b**) MKL-1 cells comparing WT with inducible TA knockdown (shTA) cells. (**c**) Cell proliferation ratio between Waga shTA and WaGa WT GFP cells over time. Cells were treated with 5 µM BRD4770 after 5 days of Dox shTA induction. (**d**) Viability of the WaGa cells was measured by MTS assay after 48 hours of EHMT2 inhibition and 24 hours of treatment with etoposide at different concentrations. Dox, doxycycline; EHMT2, euchromatic histone lysine methyltransferase 2; MTS, tetrazolium inner salt; shTA, T antigen−targeted short hairpin RNA; tLT, truncated large T antigen; VP-MCC, virus positive MCC; w/o, without; w/wo, with/without; WT, wild-type.

ARTICLE IN PRESS

K Bachiri et al.
DNA Damage Control by tLT and EHMT2 Is Central in MCC

Figure 5. Analysis of the involvement of EHMT2 and tLT in DDR. (**a**) Immunofluorescence imaging of γH2Ax loci in WaGa WT and shTA cells after treatment with 1 μM etoposide for 24 hours, 5 μM BRD4770 for 48 hours, or combined treatment with 5 μM BRD4770 for 48 hours and 1 μM etoposide for 24 hours. Bar = 50 μm. (**b**). Graphic representation of γH2Ax loci number for each condition. (**c, d**) Western blotting of several DDR markers in (**c**) WaGa or (**d**) MKL-1 WT and inducible TA shRNA cells with and without EHMT2 inhibition. The cells were also treated with 2 mM to induce replicative stress and were harvested either directly after 4 hours of HU treatment or after 18 hours of recovery. (**e**) Graphic representation of the OTM obtained by Comet assay on WaGa WT and shTA cells with and without EHMT2 inhibition. The cells were also treated with 2 mM HU to induce replicative stress and were analyzed either directly after the 4 hours of HU treatment or after 18 hours of recovery. DDR, DNA damage response; EHMT2, euchromatic histone lysine methyltransferase 2; h, hour; HU, hydroxy urea; OTM, olive tail moment; pATM, phosphorylated ataxia telangiectasia mutated; pATR, phosphorylated ataxia telangiectasia mutated and RAD3-related; pCHK, phosphorylated CHK; shTA, T antigen−targeted short hairpin RNA; TA, T antigen; tLT, truncated large T antigen; WT, wild-type.
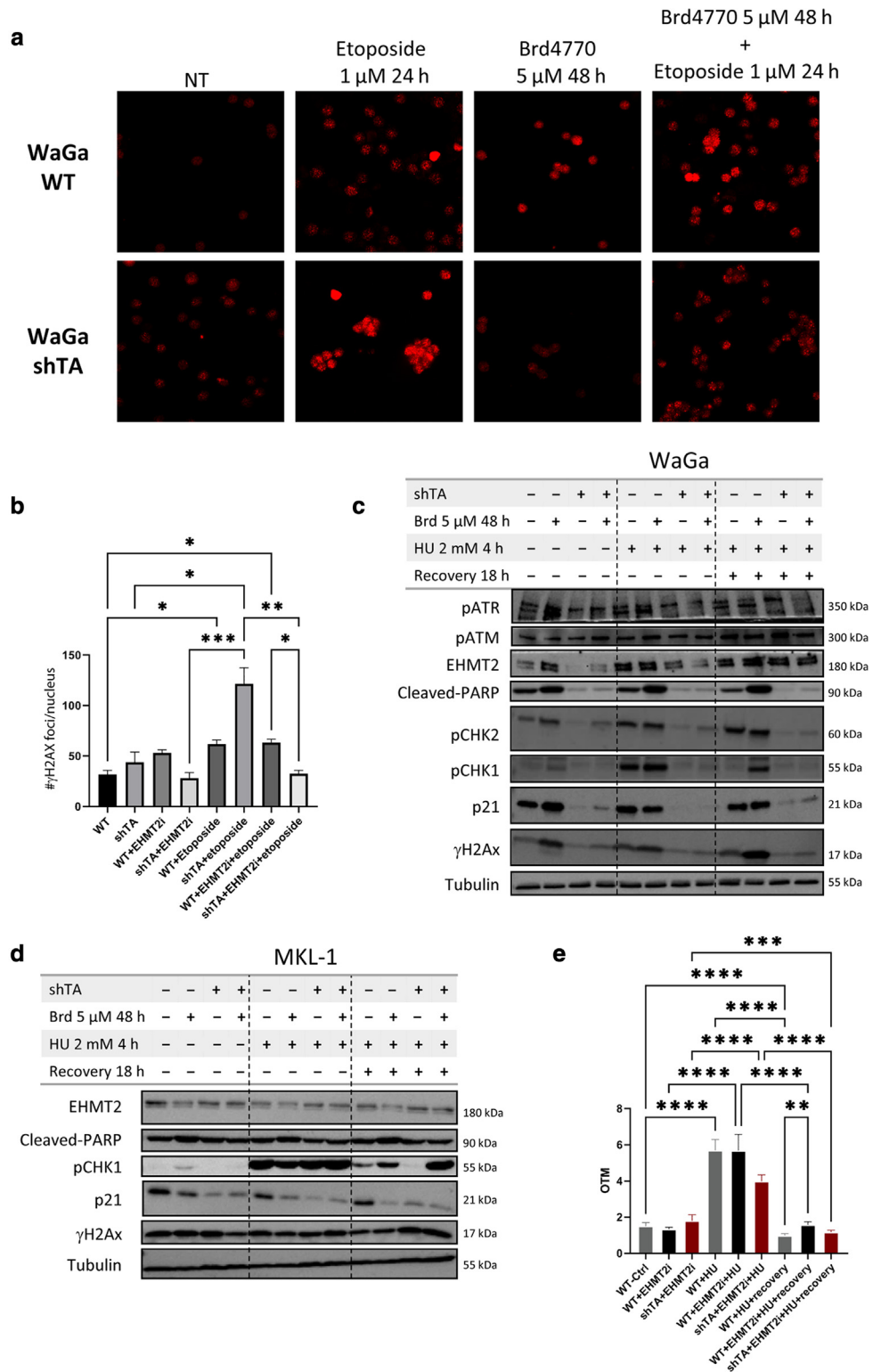
BRD4770 led to different outcomes depending on TA expression. In the cells expressing normal TAs levels, EHMT2 inhibition triggered an increase in γH2AX foci number, whereas we detected a slight decrease in cells with TA knockdown (Figure 5a and b). This result indicates that TA expression is essential for EHMT2 inhibitor (but not for etoposide)−induced DNA damage in MCC cells.

To investigate the impact of EHMT2 on the DDR, we determined the relative status of DDR markers for the different conditions. We induced the TA shRNA expression for 7 days and then treated the WaGa/MKL-1/PeTa WT and WaGa/MKL-1/PeTa inducible TA shRNA cells with 5 μM of BRD4770. We observed a trend of decreased γH2Ax levels in the WaGa TA-targeted shRNA conditions, suggesting a

ARTICLE IN PRESS

K Bachiri et al.
DNA Damage Control by tLT and EHMT2 Is Central in MCC

lower activity of the DDR signaling than in WT WaGa cells (Figure 5c). However, this was not the case for MKL-1 and PeTa cells (Figure 5d and Supplementary Figure S3b), potentially revealing differential involvement of tLT in actual basal levels of DNA damages across cell lines. We also observed more phosphorylated CHK2 in both the WT- and TA-targeted shRNA−induced condition upon EHMT2 inhibition in WaGa cells (Figure 5c). The inhibition of EHMT2 seems to activate or lift the inhibition of the DDR signaling after replication stress or SSBs.

EHMT2 and tLT cooperatively regulate the DDR pathways

EHMT2 is linked to the DDR machinery, and its inhibition impairs proper DDR, with H3K9me2 being potentially required for proper DNA repair (Gursoy-Yuzugullu et al, 2017). EHMT2 can also play a role in replication proteins A recruitment at DNA double-strand breaks in a methylation-dependent manner (Yang et al, 2017).

We assayed the ability of the VP-MCC cell line WaGa to trigger an efficient DDR. We evaluated the status of DDR markers after TA knockdown, EHMT2 inhibition, and upon induction of replicative stress by hydroxy urea (HU) treatment, with/without recovery time (Figure 5c). HU is used to initiate replication stress that induces SSB (Ercilla et al, 2020; Petermann et al, 2010). The analysis before recovery aims at assessing the possibility of the cells to trigger the DDR, and after the recovery, it is aimed at testing their ability to recover from SSB.

Analyzing DDR markers, we observed that in parental WaGa cells, EHMT2 inhibition alone led to an increase of DDR signaling, as shown by increased phosphorylated ATM and RAD3-related, phosphorylated CHK1, phosphorylated CHK2, p21, and γH2Ax levels (Figure 5c). Interestingly, after TA depletion, we also observed increased expression/phosphorylation of these markers (except for phosphorylated CHK1), with the difference that the increase started from a much lower level and did not reach that of untreated parental WaGa cells (Figure 5c). TA knockdown also led to decreased EHMT2 protein levels, whereas EHMT2 methyltransferase inhibition caused an accumulation of EHMT2. As expected, the treatment with the replicative stress inducer HU led to an increase of all analyzed DDR markers, but again, the levels in TA-depleted cells did not reach that of untreated parental cells. Interestingly, it also caused an accumulation of EHMT2. Indeed, the highest EHMT2 level was observed after 18 hours of recovery after HU treatment. Moreover, we observed a strong reduction in phosphorylated CHK1 level in the WT WaGa cells after 18 hours of recovery after HU treatment, whereas its level was still high when EHMT2 was inhibited, suggesting that EHMT2 inhibition leads to a sustained activation of DNA damage signaling as shown by high CHK1 phosphorylation. This result indicates that EHMT2 activity is required for proper DDR and recovery after replication stress induced by HU treatment. The high level of phosphorylated CHK1 after HU recovery and under EHMT2 inhibition was striking. We thus decided to assess phosphorylated CHK1 status in MKL-1 and PeTa cells under the same panel of conditions (Figure 5d and Supplementary Figure S3b). In addition to what was observed in the WaGa cells, EHMT2 inhibition also led to a sustained CHK1 phosphorylation in

inducible TA shRNA cells and not only the WT cells after HU recovery. However, MKL-1 and PeTa cells showed a decrease in p21 level after EHMT2 inhibition, whereas WaGa cells showed an increase. It was described by Gaggioli et al (2023) that EHMT2 was involved in replication stress management through trimethylation of H3K9. We thus quantified global H3K9Me3 levels under replication stress with EHMT2 and/or TA knockdown but did not observe any differences between the conditions in VP-MCC cells (data not shown). The sustained CHK1 phosphorylation when EHMT2 is inhibited could reflect defects in DNA repair and compromised genomic integrity. We then performed Comet assays to further characterize the relationship between the DDR activity and actual DNA damages and test their putative uncoupling. The olive tail moment is calculated from the Comet assay and serve as an indicator of single- and double-strand DNA breaks abundance (Figure 5e). A difference analogous to the phosphorylated CHK1 levels, which is higher in EHMT2 inhibitor−treated cells, was observed for the olive tail moment, indicating that the DNA repair was less effective upon EHMT2 inhibition and that the sustained high phosphorylated CHK1 levels could indicate the persistence of unresolved DNA damages. To monitor EHMT2 inhibition effect on apoptosis, we measured cleaved PARP levels by western blot (Figure 5c and d and Supplementary Figure S3b). Similar patterns were observed in all 3 VP-MCC cell lines. EHMT2 inhibition resulted in an increase of cleaved PARP in all the WT cells, with no effect of the HU treatment. In WaGa and PeTa, the increase of cleaved PARP levels was lower in the inducible TA shRNA cells than in the WT cells. The MKL-1 inducible TA shRNA did not display any increase in cleaved PARP under EHMT2 inhibition.

To test whether EHMT2 impact on the DDR was restricted to VP-MCC cell lines, the effects of EHMT2 inhibition were also evaluated in parental U2OS cells and U2OS cells transduced to express tLT (Supplementary Figure S4). In this context, we observed an increase in phosphorylated CHK1 levels after HU treatment (Supplementary Figure S4), indicating an effective DDR signal transmission from DNA break detection to CHK1 phosphorylation. We also observed an increase in phosphorylated CHK1 levels after EHMT2 inhibition. Interestingly, in contrast to WaGa and following the trend observed in MKL-1 and PeTa cells, the increase in CHK1 phosphorylation did not correlate with an increase of p21 expression when EHMT2 was inhibited. In the replication stress setting, that is, after HU treatment, the EHMT2 inhibition led to a strong increase in phosphorylated CHK1 levels but also a decrease in p21 total level. In this cell line, EHMT2 levels did not seem sensitive to its inhibition, HU treatment, or tLT ectopic expression.

In summary, these data strongly suggest that EHMT2 plays a role in the DDR after SSBs and/or replicative stress but that its role is cell type dependent. The constant observation across all analyzed cell lines is that EHMT2 methyltransferase activity is involved in a pathway leading to reduced CHK1 phosphorylation.

DISCUSSION

In this study, we identified EHMT2 as an important partner of tLT. tLT-dependent addressing of EHMT2 at DDR factor

ARTICLE IN PRESS

K Bachiri et al.
DNA Damage Control by tLT and EHMT2 Is Central in MCC

proximity could be central in the atypical genetic stability of MCCs and continuous growth despite replicative stress. This hypothesis is supported by the augmented abundance of DNA repair machinery factors in parental WaGa versus WaGa cells with inducible TA shRNA knockdown. Conversely, EHMT2 inhibition under these 2 settings did not change the proteomes composition, suggesting its involvement in transcription regulation—independent mechanisms.

The growth rescue upon TA knockdown of VP-MCC inducible TA shRNA cells by EHMT2 inhibition suggested a disruption of the cell cycle arrest mechanism normally after TA depletion. In addition to its role in DDR, EHMT2 methyltransferase activity inhibition was reported to increase the expression of RB1 (Rao et al, 2016). If these results were transposable to VP-MCC cell lines, EHMT2 inhibition should lead to a tight cell cycle arrest and therefore should not lead to a growth rescue. Our result suggests a more complex role of EHMT2 here, possibly involving its relation to DDR signaling after replicative stress caused by the high proliferation pace of the MCC cells.

Furthermore, we show a methyltransferase-dependent effect of EHMT2 in SSB response. In both VP-MCC and non-MCC cell lines, the inhibition of EHMT2 leads to increased levels of phosphorylated CHK1, which is a marker of SSB. Although some differences are observed between the 3 VP-MCC cell lines, they all show a higher level of phosphorylated CHK1 when EHMT2 is inhibited. In addition to this initial observation on WT cells, we noticed that in 2 of 3 VP-MCC cell lines, an increase in phosphorylated CHK1 is also observed upon TA knockdown and not only in WT cells. This could be due to an efficient induction of CHK1 phosphorylation upon HU treatment in MKL-1 and PeTa inducible TA shRNA, whereas the phosphorylated CHK1 level in WaGa cells with inducible TA shRNA knockdown seems insensitive to HU treatment. Thus, in MKL-1 and PeTa, phosphorylated CHK1 levels fail to go back to basal levels after 18 hours of recovery after HU-induced replication stress. The variations observed between the cell lines regarding p21 levels suggest a cell-type—dependent involvement of EHMT2 in p21 regulation. These results suggest that the efficiency of the DDR signal transduction through CHK1 phosphorylation is independent of EHTM2 methyltransferase function. However, the reduced DNA repair efficiency upon EHTM2 inhibitor treatment determined by Comet assays in WaGa suggests an involvement of its methyltransferase activity in DNA repair efficiency. The gH2Ax foci counts revealed a difference between the cells with and without TAs. In WaGa cells with inducible TA shRNA knockdown, we observed more gH2Ax foci than in the WT when treated with etoposide but less when treated with both etoposide and BRD4770. This difference in reaction to the combined inhibition of TAs and EHMT2 suggests a compensation of EHMT2 inhibition by the presence of the TAs. Altogether, our data show the centrality of a coordinated control of the DDR pathway by the cooperative action of tLT and EHMT2. Our experiments in the U2OS cells revealed that EHMT2 activity on the DDR pathway seems not only dependent on tLT expression but also dependent on the cellular context. This latter observation strongly suggests that additional cofactors cooperate to tune which type of activity EHMT2 would have on the DDR

pathway. Although further experiments are needed to characterize the fine EHMT2 mechanism in the DDR, our work reveals a strong interdependency of tLT and EHMT2 in DDR control, the centrality of tLT-dependent DNA damage control in MCC, and the involvement of EHMT2 in SSB signaling.

Our findings revealing a role for EHMT2 in DDR signaling and repair are consistent with a recent work by Gaggioli et al (2023) implicating EHMT2 in the protection of stalled replication forks. Specifically, they found that prolonged replication stress induced by HU led to increased trimethylation of H3K9 by EHMT2 proximal to stalled forks and described EHMT2 as a replication stress checkpoint. This increase in heterochromatic H3K9me3 marks resulted in chromatin compaction around stressed forks, which helped maintain fork integrity and prevent DNA damage. Notably, we did not observe any change in global trimethylation of H3K9 in the whole-cell lysates (data not shown). It is possible that the changes in H3K9me3 are only perceptible locally at stalled forks or DNA damage sites. Our experiments suggest an involvement of EHMT2 downstream of the DDR, whereas the study by Gaggioli et al (2023) suggests that EHMT2 could also acts upstream, during replication stress, to mediate a protective chromatin state that preserves stalled fork structure. In light of the apparent scaffolding effect of tLT on EHMT2 at the stalled replication fork, Gaggioli et al (2023)'s findings support its probable protective effect in VP-MCCs. These results indicate that EHMT2 could regulate multiple stages of the replication stress response, first, by promoting chromatin modifications that protect fork stability, and subsequently, by facilitating efficient DNA damage signaling and repair. Interestingly, we observed for all 3 VP-MCC that EHMT2 inhibition led to apoptosis induction. The increase in cleaved PARP after EHMT2 inhibition was also observed when TA expression was reduced but to a lesser extent. In line with our results, other histone methyltransferase linked to MCC oncogenesis have been recently involved in DDR. Xu et al (2019) showed in multiple myeloma that the inhibition of EZH2 was responsible for a sensitization of the cells to DNA damage. The need for DNA damage control in MCC could then explain the selective cytotoxicity of EZH2 inhibition in VP-MCC cell lines (Durand et al, 2023). The use of HKMT-1-005, an inhibitor targeting both EZH2 and EHMT2, presented synergistic effect when combined with PARP inhibitor treatment (rucaparib) in ovarian cancer cells (Garner et al, 2021). PARP inhibitors being one of the most common pharmacological tools to target DDR in cancer, this synergy highlights the potential benefit of investigating the role of histone methyltransferase in DDR and testing their inhibition for cancer treatment.

Given the development of epigenetic factors targeting drugs, these results are important to carefully consider their use in VP-MCCs and in cancer therapy in general, considering EHMT2 checkpoint role in stalled fork protection and in U2OS cell line. A recent and important body of knowledge, along with the development of small-molecule inhibitors, supports the clinical interest of targeting specific DDR components to potentiate radiotherapies, chemotherapies, and immunotherapies (reviewed in Groelly et al [2023]). Cancer cells develop—primarily or at relapse—strategies to bypass genotoxic or replicative stress through hyperactivation of 1 or

ARTICLE IN PRESS

K Bachiri et al.
DNA Damage Control by tLT and EHMT2 Is Central in MCC

several DDR pathways (Sadoughi et al, 2021). In addition, DDR targeting could potentiate immunotherapies by turning on the inflammation in tumors through micronuclei production and cGAS–STING pathway activation, facilitating the infiltration of immune cells (Concannon et al, 2023; Sen et al, 2019). Regarding therapeutic strategies, the key question is which DDR inhibitor would be the best to give to which patient. Ongoing clinical trials rely on the expression levels of canonical DDR checkpoints (eg, ATM and RAD3-related, ATM, CHK1, and WEE1). Our work suggests that EHMT2 could be of interest as a potential target in combination with immune checkpoint inhibitor or conventional chemotherapy in the VP-MCC context. The discrepancies observed between the 3 VP-MCC cell lines at the p21 levels after EHMT2 inhibition could indicate a patient-dependent response. To investigate the potential of EHMT2 expression as a marker for adjuvant therapy, we evaluated EHMT2 expression in a previously described cohort of MCC tumors included in a tissue microarray (Kervarrec et al, 2019), with the written informed consent of the patient and within the frame of the study approved by the local Ethics Committee in Human Research of Tours (Tours, France) (approval number ID RCB2009-A01056-51). Among the 135 interpretable cases, EHMT2 expression was intense and diffuse in 42 cases (31%), low/moderate in 46 cases (34%), and absent in 47 cases (35%), with no substantial differences between VP-MCC and virus-negative MCC cases (data not shown). This suggests that the expression level of EHMT2 may serve as a potential marker for stratifying a specific patient subpopulation that could benefit from EHMT2 inhibition, particularly in VP-MCCs where tLT is likely to act as a scaffold enhancing the interaction between EHMT2 and DDR components. Finally, the recent discovery of EZH2 as a potential target in MCC suggests that dual targeting of EHMT2 and EZH2 could be an interesting approach to test in VP-MCCs because it appeared promising to treat other neoplasia (Curry et al, 2015; Ishiguro et al, 2021).

In conclusion, we report the physical and functional cooperation between tLT and EHMT2 in DNA damage repair control in VP-MCCs. On the basis of these data, we believe that targeting EHMT2 could be a promising approach to potentiate current VP-MCC therapies. Our study warrants further research down that path, such as inhibiting EHMT2 or cotargeting EHMT2 and EZH2 in patient-derived xenografts expressing different levels of EHMT2.

MATERIAL AND METHODS
Cell culture
Flp-In T-REx HEK293 and U2OS cells were grown in DMEM (Gibco) supplemented with 10% fetal bovine serum (Sigma-Aldrich), GlutaMAX, and penicillin–streptomycin (1×). VP-MCC cells WaGa and MKL-1 were grown in RPMI (Gibco) supplemented with 10% fetal bovine serum, penicillin–streptomycin, and 2 mM glutamine. The WaGa cells with inducible shRNA targeting TA have been described previously (Hesbacher et al, 2016). BioID and whole-proteome analyses are detailed in Supplementary Materials and Methods.

Western blot
Cells treated with Dox for 7 days and Brd4770 (MedChem Express, number HY-16705) for 2 days were lysed in RIPA buffer (100 mM

sodium chloride, 50 mM Tris, 5 mM EGTA, 5 mM EDTA, 100 mM sodium fluoride, 10 mM sodium pyrophosphate, 1% NP-400, 1 mM phenylmethylsulfonyl fluoride) supplemented with protease inhibitor cocktail (Sigma-Aldrich). Sample preparation and analysis and the antibodies used are described in Supplementary Materials and Methods.

Confocal microscopy
In brief, cells were cultivated in labtek chambers coated with poly-lysine and subsequently rinsed using PBS. They were then fixed, washed, and permeabilized. After DAPI and anti-gH2Ax labeling (details in Supplementary Materials and Methods), images were acquired with similar exposure parameters on a Zeiss LSM700 confocal microscope, processed using the Zeiss Zen 2 software, assembled, and analyzed under ImageJ.

Proximity ligation assay
Cells were incubated in blocking solution of 1% PBS/BSA and, afterward, incubated with antibody solution overnight at 4 °C. The antibodies were diluted in resuspension buffer provided in the proximity ligation assay kit (Sigma-Aldrich, number DUO92101). The antibody used and their dilutions are as follows: anti–LT-MCPyV (Santa Cruz Biotechnology, number sc-136172, 1:200) and anti-EHMT2 (Cell Signaling Technology, number 3306s, 1:200). The proximity ligation assay was performed according to the kit provider's instructions. Images were acquired using the same process as described in the section on confocal microscopy.

Proliferation assay
WaGa, MKL-1, A375, and HEK293 cell lines were treated with increasing doses of BRD4770, and viability profile of each cell line was assessed by tetrazolium inner salt assay (Supplementary Figure S1). The half-maximal inhibitory concentration of BRD4770 in WaGa cells was calculated as described in Supplementary Materials and Methods. Cells were treated with Dox at 2 μg/ml for 5 days and seeded in 96-well plate before being treated or not with BRD4770 (MedChemExpress, number HY-16705) and UNC0642 (MedChemExpress, number HY-13980). For the matrix displayed in Figure 4b, etoposide (MedChemExpress, number HY-13629) was added or not to the wells. After 24 hours, 10 μl of the CellTiter 96 AQueous One Solution Reagent (Promega, number G3580) were added, and the absorbance was read after 2.5 hours of incubation in the dark at 37 °C.

Mixed cell culture assay
Growth behavior was compared between WaGa cells with inducible TA-targeted shRNA expression and WaGa with constitutive GFP expression. WaGa TA-targeted shRNA cells were mixed with approximately 30% of WaGa GFP. The changes in abundances between the 2 populations were recorded using flux cytometry. The cells were treated or not with Dox on day 0 and treated or not with 5 μM BRD4770 starting at day 6 of Dox treatment; BRD4770 was added every 48 hours after that initial treatment.

Comet assay
Alkaline comet tests were conducted using 2×10^5 cells, following previously established protocols (Trapp-Fragnet et al, 2014). An Axiovert 200 M inverted epifluorescence microscope (Zeiss) was used to visualize the comets, and photographs were captured with an Axiocam MRm device (Zeiss). At least 50 comets were examined for each sample through the CometScore tool (version 1.5, TriTek). The metric of the olive tail moment was calculated on the basis of

ARTICLE IN PRESS

K Bachiri et al.
DNA Damage Control by tLT and EHMT2 Is Central in MCC

the tail's length and the percentage of content DNA. Data are represented as the average olive tail moment plus/minus SD.

ORCIDs
Kamel Bachiri: http://orcid.org/0000-0003-0297-0521
Diala Kantar: http://orcid.org/0000-0001-9723-7204
Estelle M. N. Laurent: http://orcid.org/0000-0002-6138-2992
Pauline Gaboriaud: http://orcid.org/0000-0002-9740-0785
Laurine Durand: http://orcid.org/0000-0002-7824-9952
Aurélie Drouin: http://orcid.org/0000-0003-1004-9513
Mélanie Chollot: http://orcid.org/0009-0009-5779-7747
David Schrama: http://orcid.org/0000-0002-6931-8194
Roland Houben: http://orcid.org/0000-0003-4538-2324
Thibault Kervarrec: http://orcid.org/0000-0002-2201-6914
Laëtitia Trapp-Fragnet: http://orcid.org/0000-0002-5611-4977
Antoine Touzé: https://orcid.org/0000-0002-9856-9945
Etienne Coyaud: http://orcid.org/0000-0002-5893-4557

CONFLICT OF INTEREST
The authors state no conflict of interest.

AUTHOR CONTRIBUTIONS
Conceptualization: KB, DS, RH, TK, AT, EC; Formal Analysis: KB, DK, LT-F, AT, EC; Funding Acquisition: AT, EC; Investigation: KB, DK, EMNL, PG, LD, AD, MC, LT-F; Resources: DS, RH, TK, LT-F, AT, EC; Supervision: AT, EC; Validation: KB, DK, EMNL, PG, LD, AD, MC, LT-F; Writing - Original Draft Preparation: KB, DK, AT, EC; Writing - Review and Editing: KB, DS, RH, TK, AT, EC

SUPPLEMENTARY MATERIAL
Supplementary material is linked to the online version of the paper at www.jidonline.org, and at https://doi.org/10.1016/j.jid.2024.04.034.

REFERENCES

An P, Sáenz Robles MT, Pipas JM. Large T antigens of polyomaviruses: amazing molecular machines. Annu Rev Microbiol 2012;66:213—36.

Angermeyer S, Hesbacher S, Becker JC, Schrama D, Houben R. Merkel cell polyomavirus-positive Merkel cell carcinoma cells do not require expression of the viral small T antigen. J Invest Dermatol 2013;133:2059—64.

Ayrapetov MK, Gursoy-Yuzugullu O, Xu C, Xu Y, Price BD. DNA double-strand breaks promote methylation of histone H3 on lysine 9 and transient formation of repressive chromatin. Proc Natl Acad Sci USA 2014;111: 9169—74.

Becker JC, Stang A, Hausen AZ, Fischer N, DeCaprio JA, Tothill RW, et al. Epidemiology, biology and therapy of Merkel cell carcinoma: conclusions from the EU project IMMOMEC. Cancer Immunol Immunother 2018;67: 341—51.

Cheng J, Park DE, Berrios C, White EA, Arora R, Yoon R, et al. Merkel cell polyomavirus recruits MYCL to the EP400 complex to promote oncogenesis. PLoS Pathog 2017;13:e1006668.

Concannon K, Morris BB, Gay CM, Byers LA. Combining targeted DNA repair inhibition and immune-oncology approaches for enhanced tumor control. Mol Cell 2023;83:660—80.

Curry E, Green I, Chapman-Rothe N, Shamsaei E, Kandil S, Cherblanc FL, et al. Dual EZH2 and EHMT2 histone methyltransferase inhibition increases biological efficacy in breast cancer cells. Clin Epigenetics 2015;7: 84.

Durand MA, Drouin A, Mouchard A, Durand L, Esnault C, Berthon P, et al. Distinct regulation of EZH2 and its repressive H3K27me3 mark in polyomavirus-positive and -Negative Merkel cell carcinoma. J Invest Dermatol 2023;143:1937—46.e7.

Ercilla A, Feu S, Aranda S, Llopis A, Brynjólfsdóttir SH, Sørensen CS, et al. Acute hydroxyurea-induced replication blockade results in replisome components disengagement from nascent DNA without causing fork collapse. Cell Mol Life Sci 2020;77:735—49.

Feng H, Shuda M, Chang Y, Moore PS. Clonal integration of a polyomavirus in human Merkel cell carcinoma. Science 2008;319:1096—100.

Gaggioli V, Lo CSY, Reverón-Gómez N, Jasencakova Z, Domenech H, Nguyen H, et al. Dynamic de novo heterochromatin assembly and disassembly at replication forks ensures fork stability. Nat Cell Biol 2023;25: 1017—32.

Garner IM, Su Z, Hu S, Wu Y, McNeish IA, Fuchter MJ, et al. Abstract 2066: Modulation of homologous recombination repair pathway gene expression by a dual EZH2 and EHMT2 histone methyltransferase inhibitor and synergy with PARP inhibitors in ovarian cancer. Cancer Res 2021;81: 2066.

Gartin AK, Frost TC, Cushman CH, Leeper BA, Gokhale PC, DeCaprio JA. Merkel cell carcinoma sensitivity to EZH2 inhibition is mediated by SIX1 derepression. J Invest Dermatol 2022;142:2783—92.e15.

Ginjala V, Rodriguez-Colon L, Ganguly B, Gangidi P, Gallina P, Al-Hraishawi H, et al. Protein-lysine methyltransferases G9a and GLP1 promote responses to DNA damage. Sci Rep 2017;7:16613.

Goh G, Walradt T, Markarov V, Blom A, Riaz N, Doumani R, et al. Mutational landscape of MCPyV-positive and MCPyV-negative Merkel cell carcinomas with implications for immunotherapy. Oncotarget 2016;7:3403—15.

Gravemeyer J, Spassova I, Verhaegen ME, Dlugosz AA, Hoffmann D, Lange A, et al. DNA-methylation patterns imply a common cellular origin of virus- and UV-associated Merkel cell carcinoma. Oncogene 2022;41:37—45.

Groelly FJ, Fawkes M, Dagg RA, Blackford AN, Tarsounas M. Targeting DNA damage response pathways in cancer. Nat Rev Cancer 2023;23: 78—94.

Gursoy-Yuzugullu O, Carman C, Serafim RB, Myronakis M, Valente V, Price BD. Epigenetic therapy with inhibitors of histone methylation suppresses DNA damage signaling and increases glioma cell radiosensitivity. Oncotarget 2017;8:24518—32.

Heath M, Jaimes N, Lemos B, Mostaghimi A, Wang LC, Peñas PF, et al. Clinical characteristics of Merkel cell carcinoma at diagnosis in 195 patients: the AEIOU features. J Am Acad Dermatol 2008;58:375—81.

Hesbacher S, Pfitzer L, Wiedorfer K, Angermeyer S, Borst A, Haferkamp S, et al. RB1 is the crucial target of the Merkel cell polyomavirus Large T antigen in Merkel cell carcinoma cells. Oncotarget 2016;7: 32956—68.

Houben R, Adam C, Baeurle A, Hesbacher S, Grimm J, Angermeyer S, et al. An intact retinoblastoma protein-binding site in Merkel cell polyomavirus large T antigen is required for promoting growth of Merkel cell carcinoma cells. Int J Cancer 2012;130:847—56.

Huang J, Dorsey J, Chuikov S, Zhang X, Jenuwein T, Reinberg D, et al. G9a and Glp methylate lysine 373 in the tumor suppressor p53 [published correction appears in J Biol Chem. 2010;285:18122]. J Biol Chem 2010;285:9636—41.

Ishiguro K, Kitajima H, Niinuma T, Maruyama R, Nishiyama N, Ohtani H, et al. Dual EZH2 and G9a inhibition suppresses multiple myeloma cell proliferation by regulating the interferon signal and IRF4-MYC axis. Cell Death Discov 2021;7:7.

Kervarrec T. Evidence of an epithelial origin of Merkel cell carcinoma. Mod Pathol 2022;35:446—8.

Kervarrec T, Aljundi M, Appenzeller S, Samimi M, Maubec E, Cribier B, et al. Polyomavirus-positive Merkel cell carcinoma derived from a trichoblastoma suggests an epithelial origin of this Merkel cell carcinoma. J Invest Dermatol 2020a;140:976—85.

Kervarrec T, Samimi M, Hesbacher S, Berthon P, Wobser M, Sallot A, et al. Merkel cell polyomavirus T antigens induce Merkel cell-like differentiation in GLI1-expressing epithelial cells. Cancers (Basel) 2020b;12:1989.

Kervarrec T, Tallet A, Miquelestorena-Standley E, Houben R, Schrama D, Gambichler T, et al. Diagnostic accuracy of a panel of immunohistochemical and molecular markers to distinguish Merkel cell carcinoma from other neuroendocrine carcinomas. Mod Pathol 2019;32:499—510.

ARTICLE IN PRESS

K Bachiri et al.
DNA Damage Control by tLT and EHMT2 Is Central in MCC

Kwun HJ, Shuda M, Camacho CJ, Gamper AM, Thant M, Chang Y, et al. Restricted protein phosphatase 2A targeting by Merkel cell polyomavirus small T antigen. J Virol 2015;89:4191—200.

Leiendecker L, Jung PS, Krecioch I, Neumann T, Schleiffer A, Mechtler K, et al. LSD1 inhibition induces differentiation and cell death in Merkel cell carcinoma. EMBO Mol Med 2020;12:e12525.

Park DE, Cheng J, McGrath JP, Lim MY, Cushman C, Swanson SK, et al. Merkel cell polyomavirus activates LSD1-mediated blockade of non-canonical BAF to regulate transformation and tumorigenesis. Nat Cell Biol 2020;22:603—15.

Petermann E, Orta ML, Issaeva N, Schultz N, Helleday T. Hydroxyurea-stalled replication forks become progressively inactivated and require two different RAD51-mediated pathways for restart and repair. Mol Cell 2010;37:492—502.

Rao VK, Ow JR, Shankar SR, Bharathy N, Manikandan J, Wang Y, et al. G9a promotes proliferation and inhibits cell cycle exit during myogenic differentiation. Nucleic Acids Res 2016;44:8129—43.

Roux KJ, Kim DI, Raida M, Burke B. A promiscuous biotin ligase fusion protein identifies proximal and interacting proteins in mammalian cells. J Cell Biol 2012;196:801—10.

Sadoughi F, Mirsafaei L, Dana PM, Hallajzadeh J, Asemi Z, Mansournia MA, et al. The role of DNA damage response in chemo- and radio-resistance of cancer cells: can DDR inhibitors sole the problem? DNA Repair (Amst) 2021;101:103074.

Sen T, Rodriguez BL, Chen L, Corte CMD, Morikawa N, Fujimoto J, et al. Targeting DNA damage response promotes antitumor immunity through STING-mediated T-cell activation in small cell lung cancer. Cancer Discov 2019;9:646—61.

Shuda M, Chang Y, Moore PS. Merkel cell polyomavirus-positive Merkel cell carcinoma requires viral small T-antigen for cell proliferation. J Invest Dermatol 2014;134:1479—81.

Silling S, Kreuter A, Gambichler T, Meyer T, Stockfleth E, Wieland U. Epidemiology of Merkel cell polyomavirus infection and Merkel cell carcinoma. Cancers (Basel) 2022;14:6176.

Sirbu BM, McDonald WH, Dungrawala H, Badu-Nkansah A, Kavanaugh GM, Chen Y, et al. Identification of proteins at active, stalled, and collapsed replication forks using isolation of proteins on nascent DNA (iPOND) coupled with mass spectrometry. J Biol Chem 2013;288:31458—67.

Srivastava M, Chen Z, Zhang H, Tang M, Wang C, Jung SY, et al. Replisome dynamics and their functional relevance upon DNA damage through the PCNA interactome. Cell Rep 2018;25:3869—83.e4.

Tachibana M, Sugimoto K, Nozaki M, Ueda J, Ohta T, Ohki M, et al. G9a histone methyltransferase plays a dominant role in euchromatic histone H3 lysine 9 methylation and is essential for early embryogenesis. Genes Dev 2002;16:1779—91.

Trapp-Fragnet L, Bencherit D, Chabanne-Vautherot D, Le Vern Y, Remy S, Boutet-Robinet E, et al. Cell cycle modulation by Marek's disease virus: the tegument protein VP22 triggers S-phase arrest and DNA damage in proliferating cells. PLoS One 2014;9:e100004.

Ueda J, Tachibana M, Ikura T, Shinkai Y. Zinc finger protein wiz links G9a/GLP histone methyltransferases to the co-repressor molecule CtBP. J Biol Chem 2006;281:20120—8.

Watanabe S, Iimori M, Chan DV, Hara E, Kitao H, Maehara Y. MDC1 methylation mediated by lysine methyltransferases EHMT1 and EHMT2 regulates active ATM accumulation flanking DNA damage sites. Sci Rep 2018;8:10888.

Wu H, Chen X, Xiong J, Li Y, Li H, Ding X, et al. Histone methyltransferase G9a contributes to H3K27 methylation in vivo. Cell Res 2011;21:365—7.

Xu L, Tang H, Wang K, Zheng Y, Feng J, Dong H, et al. Pharmacological inhibition of EZH2 combined with DNA-damaging agents interferes with the DNA damage response in MM cells. Mol Med Rep 2019;19:4249—55.

Yang Q, Zhu Q, Lu X, Du Y, Cao L, Shen C, et al. G9a coordinates with the RPA complex to promote DNA damage repair and cell survival. Proc Natl Acad Sci USA 2017;114:E6054—63.

Yu Y, Song C, Zhang Q, DiMaggio PA, Garcia BA, York A, et al. Histone H3 lysine 56 methylation regulates DNA replication through its interaction with PCNA. Mol Cell 2012;46:7—17.

Yuan Y, Wang Q, Paulk J, Kubicek S, Kemp MM, Adams DJ, et al. A small-molecule probe of the histone methyltransferase G9a induces cellular senescence in pancreatic adenocarcinoma. ACS Chem Biol 2012;7:1152—7.

ARTICLE IN PRESS

K Bachiri et al.
DNA Damage Control by tLT and EHMT2 Is Central in MCC

SUPPLEMENTARY MATERIALS AND METHODS

Cell culture

The Flp-In system was used to create stable cell lines expressing in an inducible way either BirA* alone, truncated large T antigen (330 amino acid), or euchromatic histone lysine methyltransferase 2 N- or C-terminally tagged with BirA*Flag. The cells were generated through cotransfection of pOG44 and pcDNA5 FRT/TO BirA*Flag-bait protein gene plasmid. The selection was done in complete DMEM supplemented with 200 μg/ml hygromycin B. BioID of BirA* tagged euchromatic histone lysine methyltransferase 2 was performed using transient transfection of pcDNA5 FRT/TO BirA*Flag-euchromatic histone lysine methyltransferase 2 into cells expressing either a Flag alone or truncated large T antigen (330 amino acid) N-terminally tagged with a Flag.

Half-maximal inhibitory concentration calculation

The relative half-maximal inhibitory concentration in WaGa cells was calculated using GraphPad (version 10.2.1) on the basis of the dose response of BRD4770 on WaGa cells (Supplementary Figure S1). With a maximum effect of BRD4770 at 20 μM (67% of living cells, determined by tetrazolium inner salt assay), the relative half-maximal inhibitory concentration (50% of the maximum effect of the drug) was measured for $(100-[(100-67)/2]) = 83.5\%$ of living cells. Using an $(Y = bottom + [top-bottom]/[1 + (IC_{50}/X)$ ⌃ HillSlope]) equation to model the dose response, we obtained an interpolated curve $(Y = 0.3475/[(7.066/X)$ ⌃ $(-3.923) + 1) + 0.67])$, providing an X value (relative half-maximal inhibitory concentration) of 7.066 μM (4528–9604 with a 95% confidence interval), in line with the 6.3 μM reported by Yuan et al (2012). We selected a working dose of 5 μM on the basis of our data and the reported BRD4770 half-maximal effective concentration of 5 μM on MedChemExpress (https://www.medchemexpress.com/BRD4770.html).

BioID sample preparation

Subconfluent cells were incubated in complete DMEM supplemented with 1 μg/ml tetracycline (Sigma-Aldrich) and 50 μM biotin for 24 hours, harvested by scraping, pelleted, washed with cold PBS, dried, and frozen. Each cell pellet was resuspended in 5 ml of lysis buffer (50 mmol/l Tris-hydrogen chloride, pH 7.5, 150 mmol/l sodium chloride, 1 mmol/l EDTA, 1 mmol/l EGTA, 1% Triton X-100, 0.1% SDS, 1:500 protease inhibitor cocktail [Sigma-Aldrich], 1:1000 turbonuclease [Accelagen]), incubated on an end-over-end rotator at 4 °C for 1 hour, briefly sonicated to disrupt any visible aggregates, and then centrifuged at 45,000*g* for 30 minutes at 4 °C. Twenty-five microliters of packed, preequilibrated streptavidin Ultralink Resin (Pierce) were added, and the mixture was incubated for 3 hours at 4 °C with end-over-end rotation. Beads were pelleted by centrifugation at 500*g* for 2 minutes and washed once with 1 ml lysis buffer and 5 times with 1 ml of 50 mmol/l ammonium bicarbonate (pH = 8.3). Tryptic digestion was performed by incubating the beads with 1 μg MS-grade TPCK trypsin (Promega) dissolved in 200 μl of 50 mmol/l ammonium bicarbonate (pH 8.3) overnight at 37 °C. The following morning, 0.5 μg MS-grade TPCK trypsin was added to the beads and incubated for 2 additional hours at 37 °C. After centrifugation at 500*g* for 2 minutes, the supernatant was collected and transferred to a fresh Eppendorf tube. One additional wash was performed with 200 μl of 50 mmol/l ammonium bicarbonate and pooled with the first eluate. The samples were then lyophilized and prepared for mass spectrometry.

Mass spectrometry

BioID. Lyophilized samples were resuspended in 0.1% trifluoroacetic acid solution and desalted using C18 phase (number ZTC18S096, Sigma-Aldrich). Nano liquid chromatography (easy1000, Thermo Fisher Scientific) coupled to mass spectrometry (Q-Exactive, Thermo Fisher Scientific) was used to analyze the peptides. The system was operated in positive ion mode with a linear gradient of acetonitrile (2–30%) in 0.1% formic acid over 140 minutes at a flow rate of 300 nl/minute. Data-dependent acquisition was performed, selecting top 10 most intense MS1 ions for fragmentation and MS2.

Whole-proteome analysis. Seven million cells treated with doxycycline for 10 days were lysed using RIPA buffer (50 mM Tris-hydrogen chloride, pH 7.5, 150 mM sodium chloride, 1 mM EDTA, 1 mM EGTA, 1% Triton X-100, 0.1% SDS, 1:100 protease inhibitor cocktail [Sigma-Aldrich]), and proteins were extracted. Filter Assisted Sample Preparation (Amicon 10 kDA, number UFC501024, Merck Millipore) and protein digestion were performed with trypsin and Lys-C proteases (number V5073, Promega). Peptides were eluted, dried, and desalted using C18 phase (number ZTC18S096, Sigma-Aldrich). Nano liquid chromatography (easy1000, Thermo Fisher Scientific) coupled to mass spectrometry (Q-Exactive, Thermo Fisher Scientific) was used to analyze the peptides. The system was operated in positive ion mode with a linear gradient of acetonitrile in 0.1% formic acid over 140 minutes. MaxQuant (version 1.6.10.43) software was used to process the data using label-free quantification (LFQ). The UniProt human reference proteome database supplemented with MC polyomavirus T antigen sequences added manually was used (downloaded in December 2021). Abundance of each identified protein was compared between all conditions on the basis of LFQ. The identification parameters of the proteins and peptides were performed with a false discovery rate at 1% and a minimum of 2 peptides per protein. The statistical analysis was performed comparing 2 conditions (3 biological replicates for each condition) using student *t*-test for each given identification.

Data analysis: BioID. The proteins were identified through comparison of tandem mass spectrometry data and the Uniprot Homo Sapiens proteome database (as of December 2021) with the aid of MaxQuant (version 1.6.10.43). The guidelines were adjusted to allow for up to 2 missed trypsin cleavages. We designated methionine oxidation and N-terminal protein acetylation as variable modifications. The software's default parameters were used for the LFQ. Regarding mass tolerance, we picked 6 ppm for mass spectrometry mode and established 20 ppm for fragmentation data to coincide with tandem mass spectrometry tolerance. The protein and peptide identification practices were conducted with a false discovery rate of 1%, requiring a

ARTICLE IN PRESS

K Bachiri et al.
DNA Damage Control by tLT and EHMT2 Is Central in MCC

minimum of 2 peptides for each protein. For the control group, the LFQ measures from the 20 control experiments (BirA* solo samples from enduring cell lines) were combined into the top 3 scores for each specific identification. This trio of values served as the benchmark for comparison with the triplicates of the viral bait proteins. The data were processed using Perseus software (version 1.6.15.0). In summary, the LFQ intensity for each specimen was downloaded into Perseus, followed by a data matrix filter that excluded potential contaminants, reversed, and those identified only by site. The data were then transformed using the $\log_2(x)$ function. Student's *t*-test was performed to compare 3 biological replicates of the bait proteins with the 3 controls. Bait with a q-value <0.01 and $\log_2$ fold change >1 were considered high-confidence interactors. For the whole-proteome analysis, the same instrumentation and software were used.
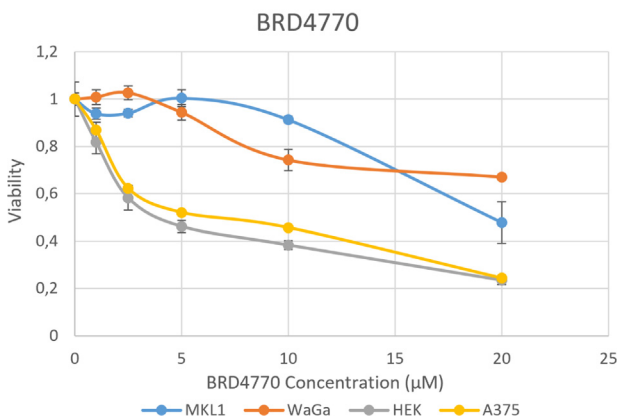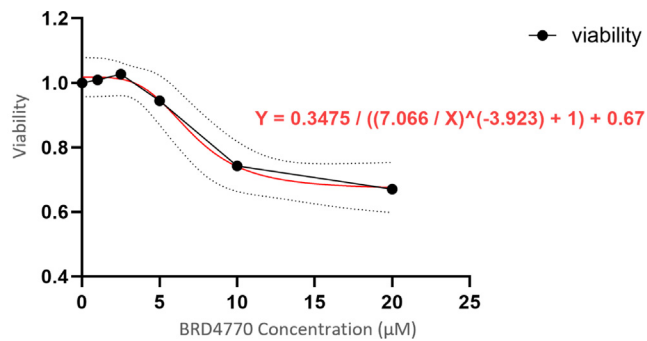
Western blot. Lysates were sonicated 2×15 seconds at 30% amplitude and centrifuged at $14,000g$ for 20 minutes at $4\,^{\circ}$C to pellet the debris; the supernatant was collected and transferred into a new tube. For each sample, protein concentration was measured using Bradford protein assay (Bio-Rad Laboratories). The concentration of the samples was homogenized, and $4 \times$ Laemmli buffer was added. SDS-PAGE migration was done using precast gels with a $4-20\%$ polyacrylamide gradient (Bio-Rad Laboratories). Immunoblotting was performed using standard protocols. The primary antibodies used were anti–phosphorylated CHK1 (Ser345) (Cell Signaling Technology, number 2348, 1/1000), anti–phosphorylated CHK2 (Thr68) (Cell Signaling Technology, number 2197, 1/1000), anti–phosphorylated ataxia telangiectasia mutated and RAD3-related (Thr1989) (Cell Signaling Technology, number 30632, 1/1000), anti–phosphorylated ataxia telangiectasia mutated (Ser1981) (Cell Signaling Technology, number 5883, 1/1000), anti-gH2Ax (Abcam, number ab2893, 1/5000), anti-p21 (Cell Signaling Technology, number 2947, 1/1000),

anti–euchromatic histone lysine methyltransferase 2 (Cell Signaling Technology, number 3306, 1/1000), anti–Merkel cell polyomavirus large T antigen (Santa Cruz Biotechnology, number sc-136172, 1/2000), and anti–proliferating cell nuclear antigen (Abcam, catalog number ab29).

Confocal microscopy. After fixation using 4% para-formaldehyde for 15 minutes at room temperature, cells were washed 3 times with PBS, and membrane perforation was done using PBS containing 0.1% Triton X-100. Blocking was performed using a solution of PBS with 0.01% Tween 20 and 5% BSA for half an hour at a temperature of $4\,^{\circ}$C. Afterward, the cells underwent an overnight incubation at $4\,^{\circ}$C with the primary antibody anti-gH2Ax (at a 1:1000 dilution, Abcam, number ab2893). After three 10-minute washes with PBS and 0.01% Tween 20, the cells were exposed to the Alexa Fluor 555–labeled secondary antibody donkey anti-rabbit IgG (H+L) (diluted 1:2000, Thermo Fisher Scientific, catalog number A-31572). A subsequent wash with PBS was performed, and cell nuclei were stained using 1 μg/ml DAPI (Thermo Fisher Scientific, number 62247) in a PBS medium for a duration of 5 minutes. After a final wash and a desalting process, slides were mounted using Dako Fluorescent Mounting Medium (Agilent Dako, Santa Clara, CA). Images were captured on a Zeiss LSM700 confocal microscope, which was linked to a Zeiss Axiovert 200 M that came with an EC Plan-Neofluar $\times 63/1.30$ numerical aperture oil immersion lens (Carl Zeiss AG, Oberkochen, Germany). Images acquisition were executed utilizing Zeiss Zen 2 software, and graphics were put together and analyzed with ImageJ (ImageJ, RRID:SCR_003070).

SUPPLEMENTARY REFERENCE

Yuan Y, Wang Q, Paulk J, Kubicek S, Kemp MM, Adams DJ, et al. A small-molecule probe of the histone methyltransferase G9a induces cellular senescence in pancreatic adenocarcinoma. ACS Chem Biol 2012;7: 1152–7.

K Bachiri et al.
DNA Damage Control by tLT and EHMT2 Is Central in MCC

$$Y = 0.3475 / ((7.066 / X)^{(-3.923)} + 1) + 0.67$$

Supplementary Figure S1. EHMT2 inhibition effect on VP-MCC and non-MCC cell lines. Upper panel: BRD4770 dose response in WaGa cells and interpolated standard curve (in red; curve formula indicated; GraphPad). Bottom panel: Proliferation of the indicated cell lines was assessed by MTS assay after 48 hours of treatment with EHMT2 inhibitor at different concentrations. EHMT2, euchromatic histone lysine methyltransferase 2; HEK, human embryonic kidney; MCC, Merkel cell carcinoma; MTS, tetrazolium inner salt; VP-MCC, virus positive Merkel cell carcinoma.
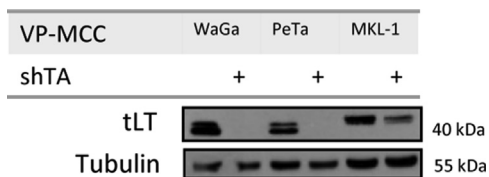

Supplementary Figure S2. WaGa, PeTa, and MKL-1 ind.TA.sh efficiency on tLT expression. Western blotting of whole-cell lysates with anti-tLT in the indicated conditions. ind.TA.sh, inducible T antigen short hairpin RNA; shTA, T antigen−targeted short hairpin RNA; tLT, truncated large T antigen; VP-MCC, virus-positive Merkel cell carcinoma.

ARTICLE IN PRESS

K Bachiri et al.
DNA Damage Control by tLT and EHMT2 Is Central in MCC
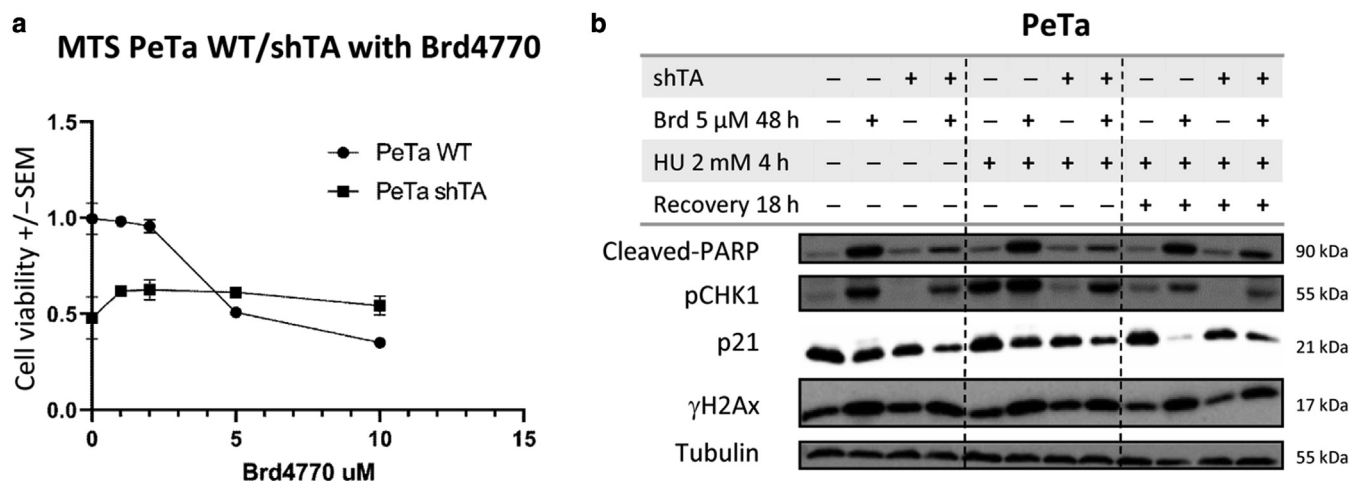
Supplementary Figure S3. EHMT2 inhibition's effect on proliferation and replication stress in PeTa cells (VP-MCC). (**a**) Proliferation of the cells was assessed by MTS assay after 48 hours of treatment with EHMT2 inhibitor at the indicated concentrations in PeTa cells with inducible T antigens knockdown. (**b**) Western blotting of several DDR markers in PeTa cells with and without EHMT2 inhibition and/or tLT expression. The cells were also treated with 2 mM HU for 4 hours to induce replicative stress and recovered 18 hours after HU treatment. DDR, DNA damage response; EHMT2, euchromatic histone lysine methyltransferase 2; h, hour; HU, hydroxy urea; MTS, tetrazolium inner salt; pCHK1, phosphorylated CHK1; shTA, T antigen–targeted short hairpin RNA; tLT, truncated large T antigen; VP-MCC, virus-positive Merkel cell carcinoma; WT, wild-type.
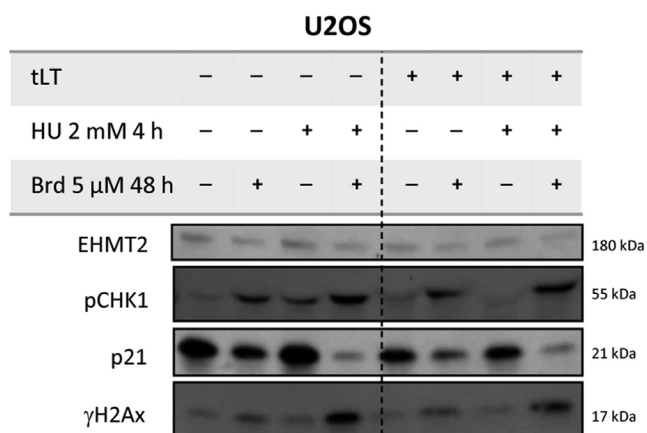
Supplementary Figure S4. EHMT2's inhibition effect on replication stress in non-MCC cell lines. Western blotting of several DDR markers in U2OS cells with and without EHMT2 inhibition and/or tLT expression was performed. The cells were also treated with 2 mM for 4 hours to induce replicative stress. DDR, DNA damage response; EHMT2, euchromatic histone lysine methyltransferase 2; h, hour; HU, hydroxy urea; pCHK1, phosphorylated CHK1; tLT, truncated large T antigen.